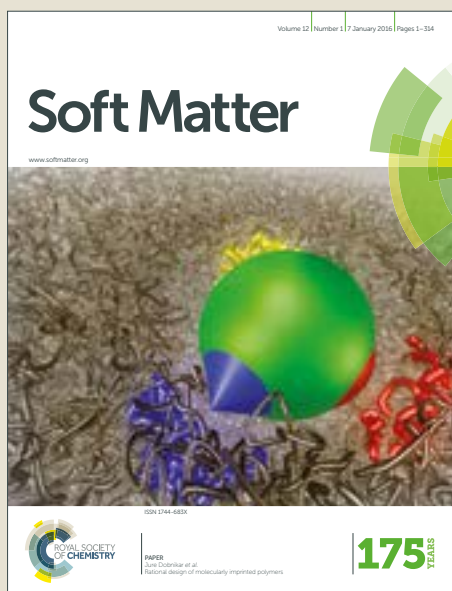


Soft Matter

Accepted Manuscript



This article can be cited before page numbers have been issued, to do this please use: A. Maity, A. Dey, M. K. Si, B. Ganguly and A. Das, *Soft Matter*, 2018, DOI: 10.1039/C8SM01071D.



This is an Accepted Manuscript, which has been through the Royal Society of Chemistry peer review process and has been accepted for publication.

Accepted Manuscripts are published online shortly after acceptance, before technical editing, formatting and proof reading. Using this free service, authors can make their results available to the community, in citable form, before we publish the edited article. We will replace this Accepted Manuscript with the edited and formatted Advance Article as soon as it is available.

You can find more information about Accepted Manuscripts in the [author guidelines](#).

Please note that technical editing may introduce minor changes to the text and/or graphics, which may alter content. The journal's standard [Terms & Conditions](#) and the ethical guidelines, outlined in our [author and reviewer resource centre](#), still apply. In no event shall the Royal Society of Chemistry be held responsible for any errors or omissions in this Accepted Manuscript or any consequences arising from the use of any information it contains.

Journal Name

ARTICLE

Impact of “half-crown/two carbonyl” - Ca²⁺ Metal Ion Interactions of a Low Molecular Weight Gelator (LMWG) on its Fiber to Nanosphere Morphology Transformation with Gel-to-Sol Phase Transition

 Received 00th January 20xx,
Accepted 00th January 20xx

DOI: 10.1039/x0xx00000x

www.rsc.org/

Arunava Maity,^{*ab} Ananta Dey,^{bc} Mrinal Kanti Si,^{bc} Bishwajit Ganguly^{*bc} and Amitava Das^{*bc}

We report here a smart functional low molecular weight gelator (LMWG) **L**, containing unusual metal ion coordination site, i.e. “half-crown/two carbonyl”. The gelator **L** shows excellent gelation behavior with typical fibrillar morphology in acetonitrile, methanol and ethanol medium. Upon Ca²⁺ ion binding with its “half-crown/two carbonyl” coordination site, the acetonitrile gel of **L** exhibit fiber to nanosphere morphology transformation along with a gel-to-sol phase transition as confirmed by microscopic investigation and by direct naked eye visualization respectively. The mechanism involved in this morphology transformation and gel-to-sol phase transition process was studied thoroughly with the help of computational calculation and various spectroscopic experiments and discussed.

Introduction

Of the options available to produce and modulate well-defined nanostructures from suitable molecular building blocks, none is more versatile than molecular self-assembly.¹ Among the various kinds of molecular assemblies, supramolecular gels based on low molecular weight gelators (LMWGs), which prevent the free movement of huge amount of solvent opposite to the gravitational force inside the entangled 3D molecular network are considered a very useful class of components to generate distinct nanostructures and for many proposed applications in a wide range of fields.² The driving forces for gelator molecules to self-assemble into entangled nanostructures are the multiple weak non-covalent interactions, such as intermolecular hydrogen (H) bonding, π - π stacking, solvophobic, Van der Waals, electrostatic, and charge-transfer (CT) interactions, metal-ligand coordination etc.³ The weak nature of these non-covalent interactions usually makes the supramolecular gels sensitive to various external stimulus (e.g. chemical agents, protons, oxidation or reduction reaction, temperature, light irradiation, sound, etc.),⁴⁻⁷ and such system provides a good platform to modulate wide variety of self-assembled structures and functions at molecular level.^{2,8} Recently to realize the straightforward

visual effect of the external stimulus on supramolecular gels, the design of gelators molecules also become an important issue. In fact, with a wide number of gelator molecules being developed and a deep understanding of their intermolecular interactions, the design of the gelator molecules shifted from serendipity to purposeful design. For instance, supramolecular gels which respond to light irradiation have been achieved by incorporating appropriate photo-responsive moieties (e.g. azobenzene, stilbene, imine, bisthiethylene and spiropyran) into the corresponding LMWGs derived from conventional gel forming functionalities.⁹⁻¹³

In the midst of various chemical stimuli applied to modify the gel behaviour, metal ions have been the most common regulators, as because of the availability and the diversity of metal-ligand coordination that could readily induce or control the self-assembly process of the gel formations.¹⁴ Sometimes this metal-ligand coordination also can induce the entrapped solvent molecules to be released, resulting in shrinking or even a gel-to-solution (sol) phase transition, and thereby influences its self-assemble nanostructures. For example, Edwards and co-workers reported the first example about gel-to-sol disassembly through Ag⁺-alkene weak interaction as the driving forces.¹⁵ Liu et al. have reported amphiphilic Schiff base organogels which exhibited different behaviors with different metal ions.¹⁶ The gel structure was disrupted when Zn²⁺ and Ni²⁺ were added. However, the gel structure was maintained in presence of Cu²⁺ and Mg²⁺ and shows twisted tape and fibrillar morphologies respectively.¹⁶ Sobczuk and co-workers displayed a gel based on crown ether appended quaterthiophene; which shows well-defined fibrillar nanostructure in alcoholic solvents. However, as in response to alkali metal cation, the fibrillar nanostructure of the

^a Organic Chemistry Division, CSIR-National Chemical Laboratory, Pune 411008, Maharashtra, India. E-mail: a.maity@ncl.res.in

^b Academy of Scientific and Innovative Research (AcSIR), New Delhi, India.

^c CSIR-Central Salt & Marine Chemicals Research Institute, Bhavnagar, 364002, Gujarat, India. E-mail: ganguly@csmcri.res.in; a.das@csmcri.res.in

† Footnotes relating to the title and/or authors should appear here.

Electronic Supplementary Information (ESI) available: [details of any supplementary information available should be included here]. See DOI: 10.1039/x0xx00000x

corresponding gelator completely vanishes upon gel-to-sol phase transition with enhanced fluorescence emission.¹⁷ Terech and co-workers reported a metallosupramolecular gel based on a multitopic cyclam and bis-terpyridine platform that showed a redox-responsive gel-to-sol phase transition and electrochromic properties.¹⁸ In addition, Deng and co-workers displayed gels of amine-modified cyclodextrins and such gels exhibited a response towards Co^{3+} , Ni^{2+} , Cu^{2+} and Ag^+ .¹⁹ In all these instances, the gelators have been deliberately designed to have various metal-binding motifs and shown the profound effects of metal-ligand coordination on the self-assembly process, self-assembled nanostructures with number of smart properties, including luminescence, redox activity etc. However, to further advance towards precise control of the self-assembly process and hence towards more complex applications, novel molecular architectures are still required.

Polyoxyethylenes, are a class of highly flexible, non-cyclic crown ether type functional group, which is known to form the complexes with metal ions (mostly alkali and alkaline earth metal ions) in the same manner as the cyclic crown ether.²⁰ Typically, these non-cyclic ether derivatives do not show a strong metal complexation ability compared to that of cyclic crown ethers.²¹ However, the flexible nature of this acyclic crown ethers allows an appreciable change in conformation of its derivatives from a linear structure to a pseudocyclic one upon the coordination with metal ions. Such conformational changes help in improving the eventual binding affinity towards metal ion.^{20,21} By taking advantage of this metal ion induced structural modulation behaviour, Nakamura and co-workers had developed a series of molecules that consisted of mono- or bis(chromophores) linked with this polyoxyethylene moiety and explored their metal ion sensing property, photo-dimerization of suitable chromophore etc.²² Usually, in this kind of molecular system, the chromophoric moiety and the complexing part, transduced the chemical information produced by metal ion binding event into an optical signal, such as colorimetric and/or fluorometric changes. Literature reports also suggest that polyoxyethylene unit is utilized as a spacer in the modulating the properties of various supramolecular and biologically active systems.²³ However, the influence of weak metal ion binding of such non-cyclic crown ether type functional moiety for transforming the self-assembled nanostructure upon gel-to-sol phase transition has seldom been reported.

Bearing in mind to expand the scope of responsiveness of the metal ion interactions with the polyoxyethylene units, herein, we design and synthesized a non-cyclic half-crown ether like gelator **L** (Fig. 1),^{23a} in which 4,7,10-trioxa-1,13-tridecanediamine is symmetrically derivatises through amide bond formation with an amide conjugate of 1-naphthalene acetic acid and L-phenylalanine (Compound 2; Scheme 1).²⁴ The gelator **L** showed translucent, homogeneous and stable organogel behavior and adopt fibrillar type morphology. It is imperative that in response to alkaline earth metal ion (Ca^{2+}), the fibrillar morphology of the **L** transform to nanospheres, which is associated with the instant gel-to-sol phase transition.

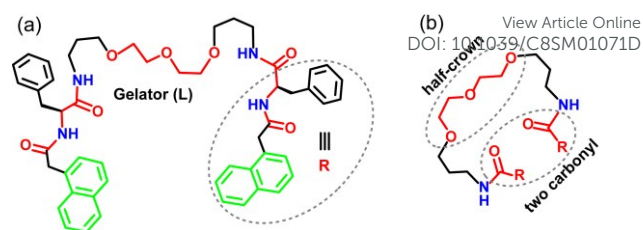


Fig. 1 (a) The molecular structure of the Gelator **L**; (b) Pictorial presentation of metal ion coordination site, which termed here as “half-crown/two carbonyl”.

The morphological transformation was confirmed by capturing the scanning electron microscopy (SEM) and transmission electron microscopy (TEM) images. The metal ion (Ca^{2+}) coordination event with the gelator **L** was investigated in detail with the help of the computational as well as with various spectroscopic studies. The computational and the experimental results reveal that the gelator molecule **L** binds with Ca^{2+} ion using its “half-crown/two carbonyl” functional motif (Fig. 1b). Apart from the Ca^{2+} ion, in response to few other alkali and alkaline earth metal ions such as Li^+ , Na^+ , K^+ , Mg^{2+} , Sr^{2+} , Ba^{2+} etc. the organogel of **L** also exhibits a “naked eye” gel-to-sol phase transition. So overall, the impact of the metal ion binding event with the “half-crown/two carbonyl” motif on the mechanism of fiber to nanosphere morphology transformation along with gel-to-sol phase transitions of the gelator **L** was presented.

Experimental section

Materials

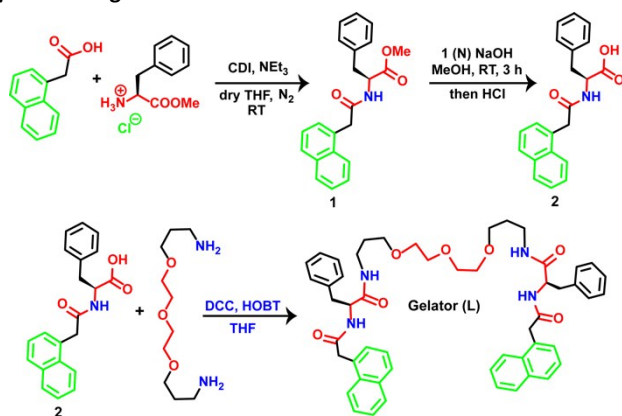
Unless otherwise stated, all reagents and organic solvents used for the synthesis of **L** were purchased from commercial suppliers and were used as such without further purification. Solvents were dried when required according to the standard procedure.²⁵ Silica gel 100-200 mesh was used for column chromatography for purifying **L** and two of its intermediate **1** and **2** (Scheme 1). HPLC grade solvents were used for gelation test and for recording the spectrometric data of the **L**.

Instruments

^1H and ^{13}C NMR spectra for the synthesized compounds were recorded on Bruker 400/500 MHz FT NMR (Model: Avance-DPX 400/500) using tetramethylsilane (TMS) as an internal standard. High-resolution mass spectra (HRMS) were recorded on JEOL JM AX 505 HA mass spectrometer. SEM images were obtained using Nova Nano SEM 450 and Quanta™ Scanning Electron Microscope. TEM images were recorded using a FEI Tecnai G2 F20 X-TWIN TEM at an accelerating voltage of 200 kV. Rheological measurements were carried out on a Rheoplus MCR302 (Anton Paar) rheometer with parallel plate geometry and obtained data were processed with start rheometer software. The gap distance between the plates was fixed at 0.5 mm. The powder X-ray diffraction (PXRD) pattern of the air-dried acetonitrile gel of **L** was recorded on a Phillips PANalytical diffractometer using $\text{Cu K}\alpha$ radiation ($\lambda = 1.5406 \text{ \AA}$).

UV-Vis absorption spectra measurements were documented using Perkin Elmer Lambda 950 UV-Vis spectrometer. All emission spectral measurements were performed using PTI Quanta Master™ steady state spectrofluorometer. Fourier transform infrared (FT-IR) transmittance spectra were recorded on a FTIR-8300 (Shimadzu) spectrometer with 2 cm⁻¹ resolution at room temperature.

Synthesis of gelator **L**



Scheme 1. Schematic presentation of the methodology that was adopted for the synthesis of gelator **L**.

Initially, the amide conjugate of 1-naphthalene acetic acid and L-phenylalanine (compound **2**, Scheme 1), an intermediate that was used for the synthesis of gelator **L**, was prepared by following a previously reported procedure.²⁴ This synthesized intermediate; compound **2** (1.0 mM) was taken in 25 mL of dry tetrahydrofuran (THF) and was cooled to 0 °C for 10 minutes under N₂ atmosphere. To this cold solution, 4,7,10-trioxa-1,13-tridecanediamine (0.5 mM) was added, followed by N,N'-dicyclohexylcarbodiimide (DCC, 1.0 mM) and 1-hydroxybenzotriazole (HOBT, 1.0 mM). The reaction mixture was stirred for about 6 hrs under the inert condition at room temperature. The progress of the reaction was monitored by TLC (eluent phase was 4 : 96; MeOH : CHCl₃). After completion of the reaction, THF was removed from the reaction mixture under vacuum and 100 ml of dichloromethane (DCM) was added to it. The DCM layer was washed with saturated NaHCO₃ (3 × 30 mL), dilute HCl (3 × 30 mL), water (3 × 30 mL) and brine solution (2 × 30 mL). This organic layer was dried over anhydrous sodium sulfate and subsequently, DCM was removed under reduced pressure to get crude **L**, which was purified by column chromatography using the 2 % MeOH in CHCl₃ gradient solvent system to give pure gelator **L** as white solid. Yield = 56 %. ¹H NMR (500 MHz, DMSO-d₆): δ (ppm) 8.43-8.42 (2H, d, J = 8, NH), 7.98-7.96 (2H, t, NH), 7.90-7.87 (4H, t, Nap-H), 7.78-7.76 (2H, d, J = 8, Nap-H), 7.49-7.46 (2H, t, Nap-H), 7.44-7.41 (2H, t, Nap-H), 7.39-7.36 (2H, t, Nap-H), 7.28-7.27 (2H, d, J = 7, Nap-H), 7.22-7.20 (10H, broad, Ar-H), 4.50-4.46 (2H, m, -CHCO), 3.90-3.88 (4H, broad, Nap-CH₂), 3.50-3.48 (4H, m, -C-CH₂-O), 3.43-3.42 (4H, m, -C-CH₂-O), 3.31-3.29 (4H, t, -N-CH₂-C), 3.11-3.05 (4H, m, -C-CH₂-O), 2.98-2.94 (2H, m, Ar-CH₂), 2.83-2.78 (2H, m, Ar-CH₂), 1.56-1.55 (4H, broad, -C-CH₂-C); ¹³C NMR (125 MHz, DMSO-d₆): δ (ppm) 170.79, 169.68, 137.71,

133.14, 132.56, 131.82, 129.07, 128.14, 127.9, 127.58, 126.82, 126.11, 125.75, 125.41, 125.29, 124.14, 69.63, 69.42, 67.80, 53.99, 37.93, 35.70, 29.03; HRMS (ESI): m/z calculated for C₅₂H₅₉N₄O₇ [M + H]⁺: 851.436, found 851.437; Elemental analysis: C₅₂H₅₈N₄O₇: C, 73.39; H, 6.87, N, 6.58., found: C, 73.26, H, 6.9, N, 6.6.

Computational methods

The conformational search of the gelator **L** and the metal ion (Ca²⁺) binding event with its 'half-crown/two carbonyl' binding motif was examined with MMFF94 (Merck Molecular Force Field) force field.²⁶⁻²⁸ The conformation search yields several conformers of gelator **L** and its corresponding complex with the Ca²⁺ ion. We have chosen the most stable conformer among them for further calculations. The conformational search has been performed using the Spartan 08 program.²⁹ Further, we considered the most stable structure from the conformational analysis and optimized the selected structure with DFT B3LYP functional using the 6-31G* basis set.³⁰⁻³² Water was employed as a solvent using SMD solvent model.³³ The vibrational frequency calculations suggest that the obtained geometry is a minimum. All calculations are performed in Gaussian 09 suite of programs.³⁴

General description of different experimental techniques

Gelation test

A weighted amount of gelator **L** was taken in a glass vial and suspended in a series of selected organic solvents (1.0 mL) and tried to dissolve by heating in closed vial condition. The hot clear solution was cooled to room temperature and then sonicated for 2-3 minutes. The system suddenly turned to a semisolid like soft mass. The "stable-to-inversion protocol of a glass vial" was adopted to ensure the gel formation. Gelation was observed in acetonitrile and alcoholic (methanol, ethanol) solvent.

Scanning electron microscopy (SEM)

A small portion of the freshly prepared acetonitrile, methanol and ethanol gel of **L** were scooped out and diluted with the respective solvents. The Resulting solutions were drop-casted on a silicon wafer and allowed to air dry for 6 hours in a dust free place. Finally, it was dried in a desiccator for overnight. Before taking images, samples were coated with gold vapor. To check the effect of Ca²⁺ metal ion coordination with **L** on its morphology, a required amount of Ca²⁺ (in acetonitrile; 2.0 equivalent) was added to the preformed acetonitrile gel of **L**. On addition of Ca²⁺, the gel turns into a solution. After 1 hour, a small portion of this subsequent solution was pipet out and diluted with acetonitrile and used for preparing the SEM sample by following the above-mentioned procedure.

Transmission electron microscopy (TEM)

The prepared samples (with and without Ca²⁺ treated); which were used for (SEM analysis), were drop-casted on carbon-coated copper grids (200 mesh) and initially allowed to air dry

for 6 hours in a dust-free place followed by under desiccator for overnight. The dried samples were employed for taking TEM images without staining.

Rheology

A freshly prepared acetonitrile gel (0.9 mg/mL) of **L** was carefully scooped out and quickly placed on the parallel plate of the rheometer to ensure minimum solvent loss through evaporation. Dynamic strain sweep tests were carried out to increase the amplitude of oscillation from 0.1% up to 100% apparent strain shear (with a frequency $\omega = 10 \text{ rad}\cdot\text{s}^{-1}$) at 25 °C. Frequency sweep experiment was performed from 0.1 to 100 rad/s at constant strain (γ) of 1 % at 25 °C.

Powder X-ray diffraction (PXRD)

A sufficient amount of acetonitrile gel of **L** was prepared in a capped glass vial. The Glass vial, containing gel was kept in uncapped condition for few days to evaporate the entrapped solvent within the gel matrix. After complete evaporation of the solvent, the air-dried solid mass was used for the PXRD study.

UV-vis and fluorescence studies

A stock solution of **L** ($1.0 \times 10^{-3} \text{ M}$) was prepared in acetonitrile, and this solution was used for all electronic and fluorescence spectral studies after appropriate dilution with acetonitrile. Except for the K^+ , the perchlorate salts of each alkali and alkaline earth metal ions (Li^+ , Na^+ , Mg^{2+} , Ca^{2+} , Sr^{2+} and Ba^{2+}) were used to prepare initially $1.0 \times 10^{-3} \text{ M}$ of stock solution in acetonitrile and used these solutions after appropriate dilution. For K^+ ion, we had used its hexafluorophosphate salt.

Fourier transform infrared (FT-IR) study

2.0 mM CD_3CN solutions of **L** (in presence and absence of 5.0 equivalent of Ca^{2+} metal ion) were used for FT-IR measurements. Approximately 60 microliters of freshly prepared appropriate sample solutions were loaded into a demountable cell consisting of two windows (CaF_2 , 3 mm thickness, Shenzen Laser), separated by a mylar spacer of 50 micrometers thickness, and FT-IR spectra were recorded. Before plotting both the FT-IR spectrum, the solvent (CD_3CN) alone spectrum was subtracted as background.

Results and discussion

The methodology that was adopted for the synthesis of gelator **L** is shown in Scheme 1. Our design strategy helped us to have the central oxyethylene spacer (half-crown) along with two carbonyl units as metal ion binding scaffold, and the two terminal amide conjugate of 1-naphthalene acetic acid and L-phenylalanine moiety (Compound **2**; Scheme 1) for favouring the self-assembly process through multiple noncovalent interactions (such as H-bonds, π - π stacking etc.) to achieve an improved gelation property.²⁴ Desired gelator molecule **L** was

isolated in pure form after necessary workup, and was characterized by various analytical/spectroscopic techniques. The pure gelator **L** was utilized for further studies.

First, the gelation ability of **L** was examined in different organic solvents (Table 1). Among various solvents, **L** was found to be sparingly soluble in acetonitrile, methanol and ethanol under ambient condition. However, it was found to dissolve completely on heating in these solvents. The hot clear solution upon cooling and subsequent sonication for 2-3 minutes, the system suddenly turned into a semisolid like soft mass, which we identified as a gel by the “stable-to-inversion protocol of a glass vial”. Fig. 2a shows the photograph of the corresponding acetonitrile gel (CGC = 0.9 wt %) of **L**, which is translucent in appearance and remained stable for a long period of time under the closed-vial condition. The resulting gel was found to be highly thermo reversible; upon heating, it was transformed into the solution and reverted to gel state after cooling to room temperature with little sonication (Fig. 2b). The gelator **L** turn into a partial gel in 1,4-dioxane and toluene, whereas it was insoluble in ethyl acetate and hexane and was found to be soluble in each of the following solvents like CH_2Cl_2 , CHCl_3 , THF, DMF and DMSO (Table 1).

Table 1 Gelation properties of **L** in different solvents.^a

Solvent	State	CGCs (wt %)
Hexane	I	-
Toluene	PG	-
Ethyl acetate	I	-
1,4-Dioxane	PG	-
DCM	S	-
CHCl_3	S	-
Acetonitrile	G	0.9 w/v
Methanol	G	1.0 w/v
Ethanol	G	1.0 w/v
THF	S	-
DMF	S	-
DMSO	S	-

^aI = insoluble, S = solution, G = gel, PG = partial gel; gel formed by heating cooling followed by slight sonication.

Following standard method “stable-to-inversion protocol of a glass vial” (Fig. 2a), it was ensured that the translucent semisolid mass was a gel. We further examined its viscoelastic behavior by rheology experiment. The viscoelastic behavior of gel is generally determined by two key parameters, elastic modulus (G' : solid-like behavior) and viscous modulus (G'' : liquid-like behavior). Fig. 2c and 2d, respectively, show the dynamic oscillatory stress sweep and a frequency sweep of the soft mass (Fig. 2a), obtained from acetonitrile. It is evident from the Fig. 2c, initially G' is higher than G'' and both accomplish a linear signature. The linear viscoelastic region (Fig. 2c), where $G' > G''$, reveals the solid character of this soft mass. Beyond the linear viscosity region at certain stress (25.02 Pa), G' falls lower than G'' , and the soft mass transforms into a liquid-like appearance (Fig. 2c). Therefore, beyond the 25.02 Pa of oscillatory stress, it begins to flow. The frequency sweep experiment, where the G' and G'' were measured as a

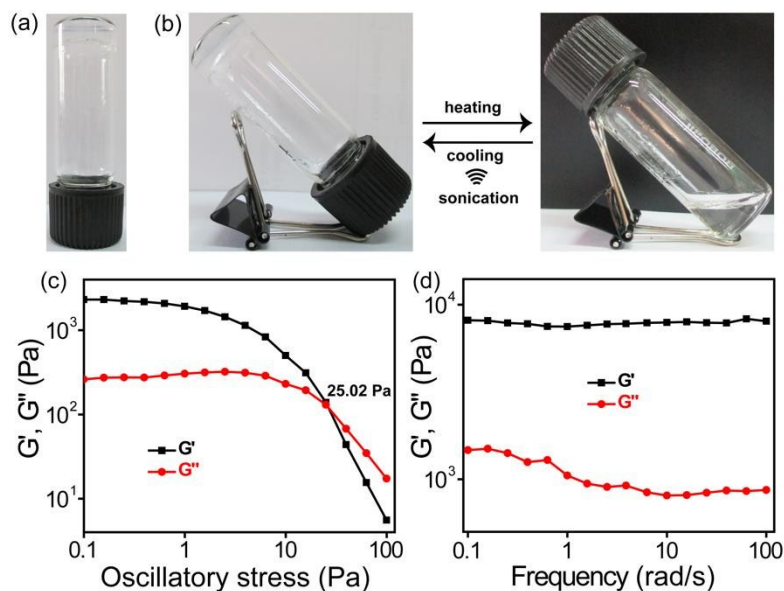


Fig. 2 Photographs showing (a) freshly prepared translucent acetonitrile gel of L and (b) its temperature induced reversible gel-to-sol transition. Dynamic oscillatory stress sweep (c) and frequency sweep (d) studies of the acetonitrile gel of L.

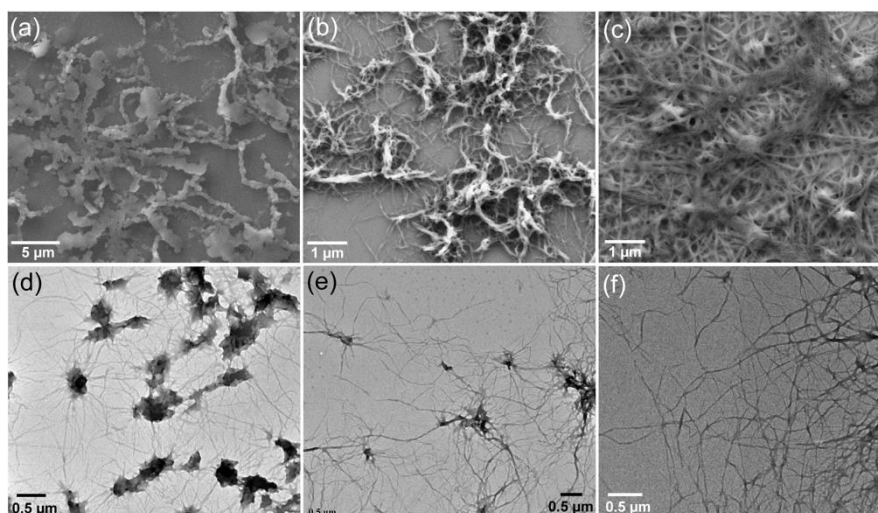


Fig. 3 (a, b, c) SEM and (d, e, f) TEM images of the diluted acetonitrile, methanol and ethanol gel of L respectively

function of angular frequency at 0.1 % constant strain, displayed the G' value of the corresponding soft mass was much higher than that of G'' for the entire of frequency range (Fig. 2d). Both G' and G'' values were found to be feebly dependent on frequency and this signified that some weak matrixes existed in it.³⁵ The higher magnitude of G' (Fig. 2d) implied that a good mechanical strength was present in this soft mass. Thus, results of the rheological experiment

confirmed that the identified semi-solid like soft mass (Fig. 2a) had a certain degree of viscoelasticity and it was actually a gelatinous material.

Next SEM and TEM experiment were performed to reveal the molecular self-assembled structures at the nanoscale level of acetonitrile, methanol and ethanol gels of L. SEM image of the dilute solution of acetonitrile gel of L showed thin plates, which were connected to each other to form flat and flexible

ribbon-like network morphology (Fig. 3a). However, SEM images of the corresponding dilute solutions obtained from methanol and ethanol gels of **L** showed entangled fibrous structures of high aspect ratio (Fig. 3b,c). Although the SEM image of the acetonitrile gel of **L** showed a thin plate-like structure, the TEM result of the same solution appeared to show well-developed fibrous network structure (Fig. 3d). The observed fibrous network consisted of entangled thin fibrils of nanometer diameter and micrometer length (Fig. 3d). Similar findings were also observed in the TEM images of methanol and ethanol gels of **L**, respectively (Fig. 3e,f). Thus, results of the SEM and TEM experiments suggest the formation of the entangled fibrillar structure as a key step for gel formation of **L**.

Presence of the “half-crown/two carbonyl” moiety^{23a} in **L** is expected to help in the binding this molecule to metal ion and influence the molecular self-assembly behavior of **L**. To examine this, we gently pipetted various equivalent amounts of Ca^{2+} ion (as its perchlorate salt) as an acetonitrile solution onto the pre-formed acetonitrile gel (0.9 wt %) of **L**. It was observed that the gel phase of **L** became unstable and a gel-to-sol transformation was induced on immediate contact of the Ca^{2+} ion. Till $[\text{Ca}^{2+}]$ was less than 1.0 mole equivalent of **L**, the acetonitrile gel of **L** existed in the partial gel state. However, for $[\text{Ca}^{2+}] \geq 1.0$ mole equivalent a complete collapse of the gel (acetonitrile gel of **L**) phase from top to bottom was observed as the Ca^{2+} salts diffused through the gel and transmuted into a homogeneous solution. Photograph of gel-to-sol phase transition of acetonitrile gel (0.9 wt %) of **L** in response to 2.0 equivalent of Ca^{2+} ion is shown in Fig. 4a. Instability of the

ions, a complete gel-to-sol phase transition was observed, as it was observed for the Ca^{2+} ion.

DOI: 10.1039/C8SM01071D

As the metal ion treatment influence the gel-to-sol phase transition, thus one might expect that self-aggregated network structure can also be affected. To examine this, SEM and TEM characterization was performed of the dilute solution of the corresponding transformed gel-to-sol solution (Fig. 4a) obtained after the addition of 2.0 equivalent of Ca^{2+} ion in acetonitrile gel of **L**. Interestingly both the SEM and TEM image of the transformed sol solution of **L** showed a spurted nanosphere architecture (Fig. 4b, 4c) with complete disappearance of their network structure, which was otherwise observed in Fig. 3a and 3d. This observation again confirms that the treatment of metal ion on the designed gelator **L** has a serious effect on its self-assembly mode, which eventually triggers its morphology transformation and gel-to-sol phase transition.

After direct visualization of morphological transition from fibrillar network to nanospheres structure microscopically and naked eye detection on gel-to-sol phase transition (Fig. 4), we were curious to find out the involved non-covalent interactions in gelator **L** and the alteration of these interactions upon complexation with Ca^{2+} and also the mode of binding of Ca^{2+} in its $\text{L}\cdot\text{Ca}^{2+}$ complex. As these are the crucial factors to determine the particular molecular arrangement in self-aggregated state and to establish the mechanism of self-assembly process. In this milieu, the solid-state single crystal structure is the ultimate proof to establish the precise molecular arrangement and envisage the operating noncovalent interactions of any assemblies in their self-assemble state. Unfortunately, despite our repeated attempts with various solvent composition and experimental condition we failed to grow a single crystal of **L** and $\text{L}\cdot\text{Ca}^{2+}$. As an alternative, we performed computational studies for **L** and $\text{L}\cdot\text{Ca}^{2+}$ using density functional theory (DFT) calculations employing the B3LYP functional and 6-31G* basis set.³⁰⁻³²

The optimized structure of the metal-free gelator **L** showed that it attained an interesting folded structure with the assistance of several intramolecular non-bonded interactions such as H-bonds between the carboxyamides and the ethereal oxygen atoms and C-H...O interaction between aromatic hydrogens and ethereal oxygens (Fig. 5a). A critical inspection of the Fig. 5a reveals that the aromatic rings of the gelator **L** interact with each other via $\text{CH}\cdots\pi$ and $\pi\cdots\pi$ interactions. The cumulative effect of these interactions, (namely intramolecular H-bonds, C-H...O, $\text{CH}\cdots\pi$ and $\pi\cdots\pi$ interactions) helped the gelator **L** to attain this folded structure (Fig. 5a). The gelator **L** also have free amide (NHCO) functional groups that can be involved in the formation of the extended intermolecular H-bond formation among the consecutive **L** molecules and eventually can result in a fibrillar network-like structure and gel formation.

The energy optimized structure of the $\text{L}\cdot\text{Ca}^{2+}$ complex is shown in Fig. 5b. In the metal-free gelator **L**, the central oxyethylene moiety was poisoned in the anti-orientation of its adjacent two carbonyl groups (Fig. 5a). However, the

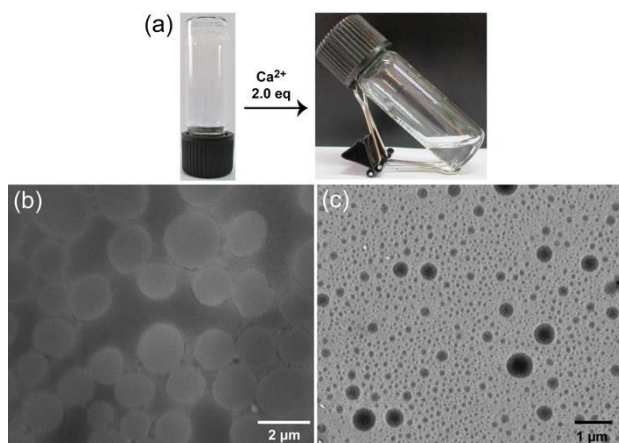


Fig. 4 (a) Gel-to-Sol phase transition of acetonitrile gel (0.9 wt %) of **L** with the addition of 2.0 equivalents of the Ca^{2+} ion; (b and c) SEM and TEM image of the corresponding transformed sol solution (after proper dilution) respectively, show the nanosphere morphology formation.

acetonitrile gel of **L** was further examined in the presence of few other alkali and alkaline earth metal ions such as Li^+ , Na^+ , Mg^{2+} , Sr^{2+} , Ba^{2+} (as their perchlorate salts) and K^+ (as the hexafluorophosphate salt). The KPF_6 is preferred over KClO_4 in our study as the latter is known to be sparingly soluble in acetonitrile; the solvent used in this study. The gel phase was retained partially in the presence of Li^+ , Na^+ , K^+ , Mg^{2+} , Sr^{2+} , Ba^{2+} metal ions having a concentration ≤ 1.0 mole equivalent of **L**. With the addition of more than 1.0 equivalent of these metal

ARTICLE

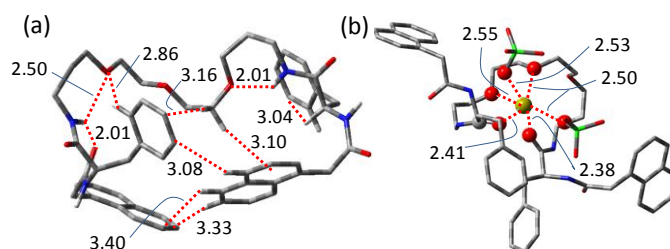


Fig 5 (a and b) The optimized structure of gelator **L** and **L•Ca²⁺** complex at B3LYP/6-31G* method in aqueous phase. Non interacted H atoms are omitted for clarity. (Color code: red = oxygen; blue = nitrogen; grey = carbon; green = chlorine; olive = calcium).

optimized metal complex structure (**L•Ca²⁺**) showed that in favor of binding with **Ca²⁺** both the carbonyl groups turned toward the same direction of the oxyethylene moiety (Fig. 5b). Due to this conformation change, gelator **L** formed a crown ether-like cavity and the **Ca²⁺** ion was encapsulated within it with the help of the coordination to the two central amide-carbonyl oxygen and two ethereal oxygen atoms of the half-crown like triethylene oxide linkage of **L** (Fig. 5b). Interestingly, two counter anions (**ClO₄⁻**) also remained bonded to the **Ca²⁺** metal ion effectively and hence the **L•Ca(ClO₄)₂** complex accomplished a 6-coordinated quasi-octahedral type geometry with **Ca²⁺...O** distances within the range of 2.38–2.55 Å (Fig. 5b). The gelator **L**, therefore, utilized its “half-crown/two carbonyl” binding motif to coordinate the **Ca²⁺** metal ion (Fig. 1b and 5b). Again, in comparison to the optimized structure of **L**, the **L•Ca(ClO₄)₂** structure shows, upon coordination of **Ca²⁺** metal ion, two naphthalene rings of **L** were positioned far away from each other and entire molecular orientation changes in such a way that all the existed non-covalent interactions (intramolecular multiple H-bonds, **CH...π** and **π...π** interactions etc.) in the metal-free gelator **L** completely disappears. Further, the electrostatic repulsion is also a common problem among the bound metal ions to a ligand, which usually hampered the intermolecular interactions among the consecutive molecules and results in their disassembly process.¹⁵ Perhaps, in our molecular system, the gelator **L** also possesses this strong charge repulsion force after the binding of **Ca²⁺** ions, which profoundly affect to disrupt the inter and intramolecular H-bonds, **CH...π** and **π...π** interactions etc. and finally leads to a dissociation of the gel phase and its fibrillar network to nanosphere morphology transition.

To gain the additional insight into the modes of molecular packing experimentally, powder X-ray diffraction (PXRD) measurement were recorded of the air-dried acetonitrile gel of **L**. In the small angle region of its PXRD pattern a peak at $2\theta = 6.39^\circ$ was observed (Fig. 6). The corresponding *d*-spacing value 13.7 Å for this peak calculated according to Bragg's equation, is closely matched with its energy optimized folded molecular

length (~ 12.607 Å, Fig. S1). This result validates the existence of the folded molecular structure (as shown in Fig. 5a) of **L** in its self-assemble state. Furthermore, in the wide angle region of the PXRD of **L** (Fig. 6) the appearance of a broad peak at $2\theta = 16.76\text{--}24.50^\circ$ ($d = 5.2\text{--}3.6$ Å) arises due to alkyl group packing and aromatic $\pi\text{--}\pi$ stacking interaction of the gelator molecules in its gel state.³⁶ However the assignment of the peak at $2\theta = 10.43^\circ$ ($d = 8.5$ Å) at present remains unsolved.

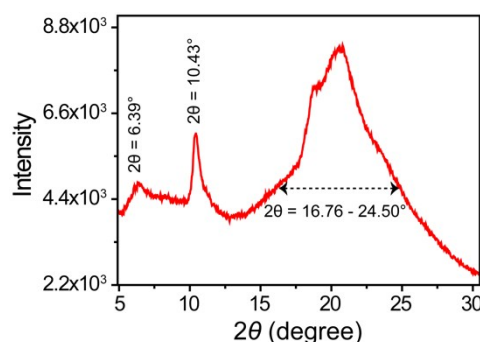


Fig. 6 Powder X-ray diffraction (PXRD) pattern of the air-dried acetonitrile gel of **L**.

To investigate the mechanism of cation response on the molecular scale, we record and analyze the FT-IR spectrum of the gelator **L** with and without **Ca²⁺** ion in **CD₃CN**. The peak at 1669 cm^{-1} was attributed to the amide carbonyl stretch (**C=O_{amide^{str}}**) of **L** in absence of metal ion (Fig. 7; blue line). The position of this peak in the IR frequency range revealed an unambiguous signature of a network of H-bonded amides of the metal-free **L**. When **Ca²⁺** was added, the corresponding amide carbonyl (**C=O_{amide^{str}}**) peak shifted to 1645 cm^{-1} (Fig. 7; red line). In presence of **Ca²⁺**, the shifting of this peak position to lower wavenumber region indicates the weakening of the **C=O_{amide}** bond strength (Fig. 7; red line). This is attributed to the **Ca²⁺** binding to **C=O_{amide}** group of **L**. It was presumed that the gel network of **L** was mainly formed through the intermolecular hydrogen bond interactions between the amide (**CONH**) groups. Binding of **Ca²⁺** to **C=O_{amide}** group was expected

to destroy this corresponding intermolecular hydrogen bonds between amide (CONH) groups within the gel networks of **L** and thus promoting its gel-to-sol transition.

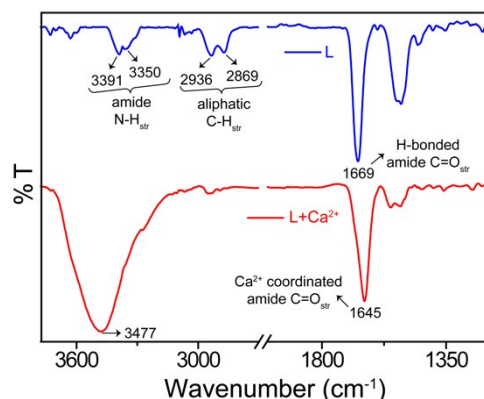


Fig. 7 FT-IR spectra of 2.0 mM CD₃CN solution of gelator **L** in the presence (red line) and absence (blue line) of 5.0 equivalent of the Ca²⁺ ion.

In higher wavenumber region, two more peaks for the N-H stretch (amide N-H^{str}) of **L** appeared at 3350 cm⁻¹ and 3391 cm⁻¹ also directs their H-bonded nature (Fig. 7; blue line). However, due to the interference of water molecule with the addition of Ca²⁺ salt, these two distinct N-H stretches of gelator **L** merged and a broad signal appeared at 3477 cm⁻¹ (Fig. 7; red line). The peaks at 2869 cm⁻¹ and 2936 cm⁻¹ for **L** were assigned to the aliphatic -C-H stretch (-C-H^{str}, Fig. 7; blue line), which also become broad and almost negligible with the addition of Ca²⁺ (Fig. 7; red line).

In order to further confirm the metal ion coordination mode of **L** in **L**•Ca(ClO₄)₂, we performed the ¹H NMR study of **L** in the absence and presence of Ca²⁺ ion in DMSO-d₆ at 298 K. Due to the low solubility and high gelatinous nature of **L** in acetonitrile, it was not possible to investigate the ¹H NMR study in CD₃CN. The partial ¹H NMR spectra of **L** before and after the addition of Ca²⁺ are shown in Fig. 8 as a typical result. Peak assignments of the important protons were made by using TOCSY NMR spectra (Fig. S2). The central oxyethylene protons of **L** (protons a, b and c; Fig. 8) showed a marginal up-field shift upon complexation to Ca²⁺. This suggests that Ca²⁺ ion was weakly coordinated to the ethereal oxygen atom. On the other hand, the amide proton (identified as 'f'; Fig. 8), neighboring to the central oxyethylene moiety, showed considerable up-field shifts ($\Delta\delta = -0.09$ ppm) when spectra were recorded in the presence of Ca²⁺. This observation suggested rather strong coordination of the Ca²⁺ ion to the two carbonyl oxygen atom (O_{C=O}). Another set of amide proton 'g' (Fig. 8) also showed a significant up-field shift upon complexation of **L** with Ca²⁺. The considerable shifts of amide protons and also the oxyethylene protons signals were associated with the structural reorganization and conformational changes of **L** during the binding of its central 'half-crown/two carbonyl' motif to Ca²⁺; an observation that was also supported by the results of the computational studies (Fig. 5). Due to the structural reorganization and conformational change upon complexation, these mentioned protons of **L** are probably covered with shielding area of

naphthalene moiety (Fig. 5), which results in their diamagnetic shifts (up-field shifts).^{22c}

DOI: 10.1039/C8SM01071D

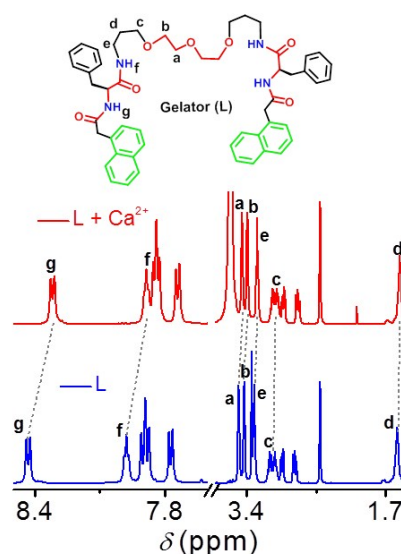


Fig. 8 Partial ¹H NMR spectra (500 MHz, 25°C) in DMSO-d₆ of gelator **L** (blue line; 20.0 mM) and after the addition of 5.0 equivalent of Ca²⁺ (red line).

The presence of chromophoric naphthalene unit in **L** further offered us an opportunity to probe the binding phenomena of Ca²⁺ ion with **L** by using the UV-Vis and fluorescence spectroscopy. The UV-Vis absorption spectrum of **L** (1.0 × 10⁻⁵ M) in acetonitrile solution at 298 K, showed band maxima at 283 nm with two shoulders at 272 and 293 nm. These were assigned to the π-π* transitions of naphthalene moiety (Fig. 9a; black line). The fluorescence spectrum of the corresponding solution showed two maxima at 328 and 337 nm (Fig. 9b; black line).

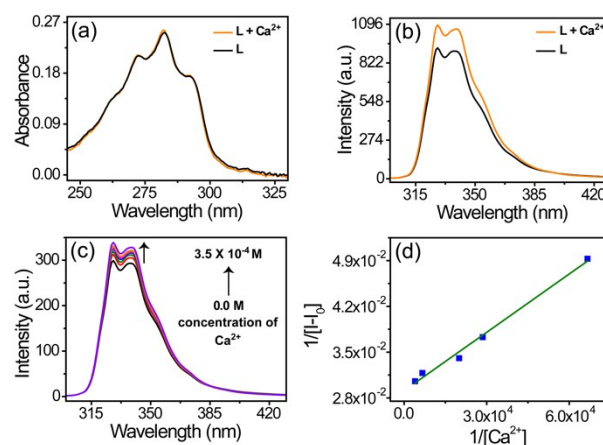


Fig. 9 Uv-Vis absorption (a) and fluorescence (b) spectra of gelator **L** (1.0 × 10⁻⁵ M) in absence (black line) and presence (orange line) of 20 mole equivalent of Ca²⁺ ion; (c) change in fluorescence spectral pattern for **L** (1.0 × 10⁻⁵ M) with varying the concentrations of Ca²⁺ (from 0.0 - 3.5 × 10⁻⁴); (d) Benesi-Hildebrand (B-H) plot of 1/[I - I₀] vs 1/[Ca²⁺]. For all studies were performed in pure acetonitrile medium, for fluorescence spectra (λ_{ex} = 283 nm).

Upon addition of 20 mole equivalent of Ca²⁺ salts in acetonitrile, failed to induce any significant change in the absorption spectrum of **L** (Fig. 9a; orange line). In contrast to the absorption spectrum, upon addition of 20 mole equivalent Ca²⁺, a little enhancement in the fluorescence intensity of **L** was obtained (Fig. 9b; orange line). The increased emission

intensity of **L** is must be due to the formation of the little bit rigid structure upon complexation with Ca^{2+} ion compared to its metal-free flexible form. To understand the binding affinity of **L** towards Ca^{2+} , systematic fluorescence titration was also carried out in acetonitrile medium with varying $[\text{Ca}^{2+}]$ ($0.0 - 3.5 \times 10^{-4} \text{ M}$), while the concentration of **L** was kept constant ($1.0 \times 10^{-5} \text{ M}$). With the increase of $[\text{Ca}^{2+}]$, a small but gradual increase of emission intensity of **L** was observed (Fig. 9c) at 328 and 337 nm. Using parameters that were obtained from this titration plot (Fig. 9c), formation constant (K_a) for **L**• Ca^{2+} was evaluated using Benesi-Hildebrand (B-H) plot (Fig. 9d), and it was found to be $(9.7 \pm 0.2) \times 10^4 \text{ M}^{-1}$. A good linear fit of the B-H plot for $1/[I - I_0]$ vs $1/[\text{Ca}^{2+}]$ confirmed the 1:1 binding stoichiometry.³⁷ Likewise B-H plot, the Jobs plot analysis also confirm a 1:1 binding stoichiometry between **L** and Ca^{2+} ion (Fig. S3). The Calculated formation constant (from B-H plot, Fig. 9d) for the **L**• Ca^{2+} complex in pure organic solvent ensured that interaction between **L** and Ca^{2+} ion was moderate.

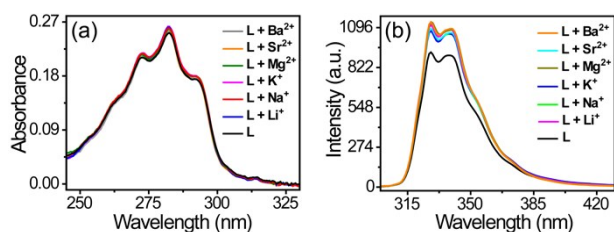
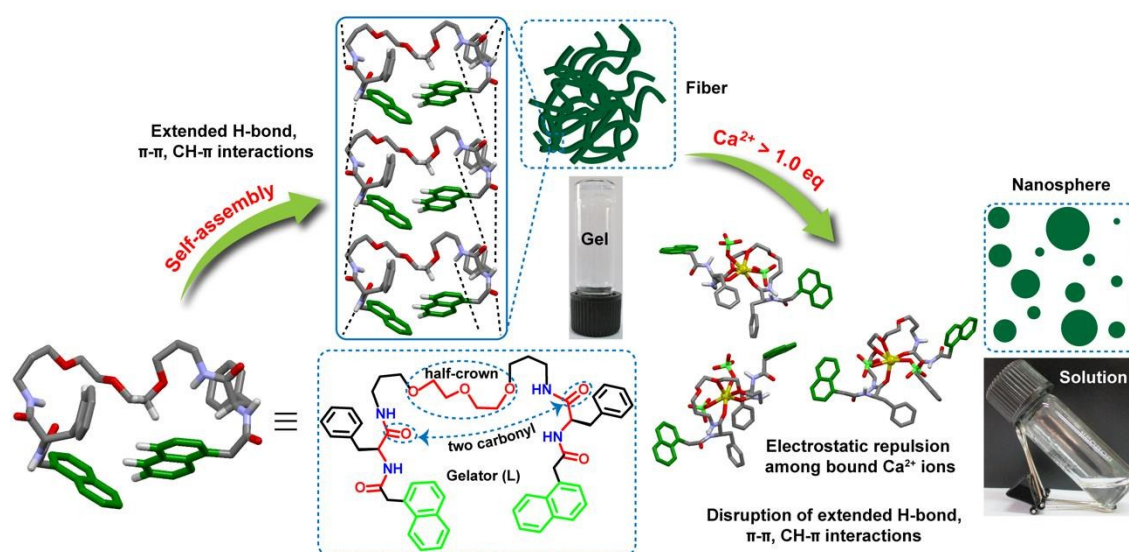


Fig. 10 (a) UV-Vis absorption, (b) fluorescence spectra of gelator **L** ($1.0 \times 10^{-5} \text{ M}$) in absence and presence of 20 mol equivalent of different alkali and alkaline earth metal ions in acetonitrile medium. For fluorescence spectra ($\lambda_{\text{ex}} = 283 \text{ nm}$).

We have also recorded both the UV-Vis absorption and fluorescence spectra of the of **L** ($1.0 \times 10^{-5} \text{ M}$) in the presence of 20 mole equivalent of other alkali and alkaline earth metal ions (such as Li^+ , Na^+ , K^+ , Mg^{2+} , Sr^{2+} and Ba^{2+}) in acetonitrile. No detectable change in absorption spectrum was observed (Fig. 10a); whereas a little increase in the emission intensity of the **L** was observed on the treatment with any one of the above-

referred metal ions (Fig. 10b). Although the UV-Vis absorption study does not give any impression on the interaction of **L** with the alkali and alkaline metal ions, the increase of emission intensity upon addition of these metal ions to the dilute solution of **L** clearly indicates metal ion coordination role is operating here

Together with the above experimental facts and theoretical calculations, it is now possible to summarize the impact of Ca^{2+} ion coordination with the “half-crown/two carbonyl” motif of **L** on the mechanism of its fiber to nanosphere morphology transformation along with gel-to-sol phase transition. Metal-free gelator **L** initially enriched with various noncovalent interactions such as intramolecular H-bonds, $\text{CH}\cdots\pi$ and $\pi\cdots\pi$ interactions (Fig. 5a and 6). Along with these intramolecular interactions, during the course of self-assembly, the consecutive **L** molecules build an extended network structure with the help of intermolecular H-bonding interactions among the amide (NHCO) groups and resulted into gel with entangled fibrillar morphology (Scheme 2). This is quite sure that the main driving force behind the fibrillar network structure is these intermolecular H-bonding interactions among the amide (NHCO) groups. Now with incorporation of Ca^{2+} ions, **L** is coordinated with the Ca^{2+} using its “half-crown/two carbonyl” binding motif, as a result the strength of the H-bond becomes weak; as the two carbonyl groups are no more available to participate in the intermolecular H-bonds, and hence the gel phase of **L** becomes unstable. Further, in favor of Ca^{2+} ion coordination, the molecular orientation of **L** also changes in a manner that the existed all intramolecular interactions disappear (Fig. 5b); this also contributes to destabilizing the self-assembled gel state of **L**. Finally, with the addition of the excess equivalent of Ca^{2+} ion, the electrostatic repulsion among the bound Ca^{2+} ions prevailed and this kept neighboring **L** molecules away from each other and disrupted the aggregated structure for **L** (Scheme 2).¹⁵ As a result, fibrillar network morphology disassembled into the basic spherical structure and gel-to-sol phase transition took place.



Scheme 2 Schematic presentation of the mechanism of fiber to nanosphere morphology transformation along with gel-to-sol transition of **L** upon “half-crown/two carbonyl”- Ca^{2+} coordination.

ARTICLE

Conclusions

In conclusion, we have introduced a relatively new kind of metal ion binding motif ("Half-crown/two carbonyl") based LMWG **L**, and established its metal ion (Ca²⁺) responsive morphological as well as gel-to-sol phase transition mechanism. We suggested that, the gel network of **L** is underpinned by intermolecular H-bonding interaction among the amide (NHCO) groups, and the disruption of these H-bonds upon binding of Ca²⁺ ion to the "Half-crown/two carbonyl" binding motif of **L** is the main driving force for the collapse of the gel phase of **L** and hence its assembled entangled fibers to disassembled nanospheres morphology transition. In quick summary, we have represented a unique example in which "Half-crown/two carbonyl" - Ca²⁺ interactions play a vital role in mediating a response in soft matter systems, providing fundamental insight into the nature of this interaction and acting as a step on the way to the development of metal-responsive materials.

Conflicts of interest

There are no conflicts to declare.

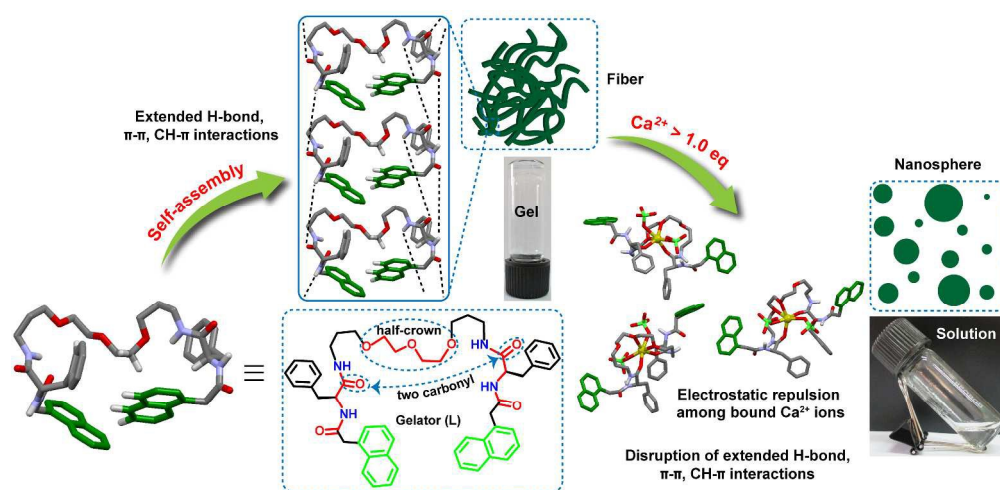
Acknowledgments

A.M. and A.D. acknowledge CSIR for their research fellowship. M.K.S is thankful to UGC, New Delhi, India for awarding a fellowship. B.G. thanks (SIP, MSM, CSIR, New Delhi, DAE-BRNS, Mumbai) and DST, New Delhi for financial support. A.D. acknowledges SERB (India) (EMR/2016/001850 and JCB/2017/000004/SSC) and DRDO (India) (ERIP/ER1502249/M/01/1685) for funding. Supports from CSIR-NCL and CSIR-CSMCR) are also gratefully acknowledged.

Notes and references

- (a) T. Aida, E. W. Meijer and S. I. Stupp, *Science*, 2012, **335**, 813; (b) X. Zhao, F. Pan, H. Xu, M. Yaseen, H. Shan, C. A. E. Hauser, S. Zhang and J. R. Lu, *Chem. Soc. Rev.*, 2010, **39**, 3480; (c) L. C. Palmer and S. I. Stupp, *Acc. Chem. Res.*, 2008, **41**, 1674; (d) G. M. Whitesides and B. Grzybowski, *Science*, 2002, **295**, 2418; (e) W. Li, Y. Kim, J. Li and M. Lee, *Soft Matter*, 2014, **10**, 5231; (f) E. Busseron, Y. Ruff, E. Moulin and N. Giuseppone, *Nanoscale*, 2013, **5**, 7098; (g) F. J. M. Hoeben, P. Jonkheijm, E. W. Meijer, A. P.H. J. Schenning, *Chem. Rev.*, 2005, **105**, 1491; (h) A. Wang, W. Shi, J. Huang and Y. Yan, *Soft Matter*, 2016, **12**, 337; (i) A. Maity, A. Dey, M. Gangopadhyay and A. Das, *Nanoscale*, 2018, **10**, 1464; (j) Y. Yan, Y. Lin, Y. Qiao and J. Huang, *Soft Matter*, 2011, **7**, 6385; (k) S. Kushwaha, A. Maity, M. Gangopadhyay, S. Ravindranathan, P. R. Rajamohan and A. Das, *Langmuir*, 2017, **33**, 10989; (l) H. Frisch, P. Besenius, *Macromol. Rapid Commun.*, 2015, **36**, 346.
- (a) P. Terech and R. G. Weiss, *Chem. Rev.*, 1997, **97**, 3133; (b) L. Zhang, X. Wang, T. Wang and M. Liu, *Small*, 2015, **11**, 1025; (c) S. S. Babu, V. K. Praveen and A. Ajayaghosh, *Chem. Rev.*, 2014, **114**, 1973; (d) L. A. Estroff and A. D. Hamilton, *Chem. Rev.*, 2004, **104**, 1201; (e) M. George and R. G. Weiss, *Acc. Chem. Res.*, 2006, **39**, 489; (f) N. M. Sangeetha and U. Maitra, *Chem. Soc. Rev.*, 2005, **34**, 821; (g) L. E. Buerkle and S. J. Rowan, *Chem. Soc. Rev.*, 2012, **41**, 6089; (h) E. R. Draper and D. J. Adams, *Chem.*, 2017, **3**, 390; (i) A. Dasgupta, J. H. Mondal and D. Das, *RSC Adv.*, 2013, **3**, 9117; (j) B. O. Okesola and D. K. Smith, *Chem. Soc. Rev.*, 2016, **45**, 4226.
- (a) A. Baral, S. Basak, K. Basu, A. Dehsorkhi, I. W. Hamley and A. Banerjee, *Soft Matter*, 2015, **11**, 4944; (b) Z. Shen, Y. Jiang, T. Wang and M. Liu, *J. Am. Chem. Soc.*, 2015, **137**, 16109; (c) A. Maity, F. Ali, H. Agarwalla, B. Anothumakkool and A. Das, *Chem. Commun.*, 2015, **51**, 2130; (d) P. Xing, P. Li, H. Chen, A. Hao and Y. Zhao, *ACS Nano*, 2017, **11**, 4206; (e) S. Datta and S. Bhattacharya, *Soft Matter*, 2015, **11**, 1945; (f) S. Ahmed, J. H. Mondal, N. Behera and D. Das, *Langmuir*, 2013, **29**, 14274; (g) A. Maity, M. Gangopadhyay, A. Basu, S. Aute, S. S. Babu and A. Das, *J. Am. Chem. Soc.*, 2016, **138**, 11113; (h) T. M. Babu and E. Prasad, *Chem. - A Eur. J.*, 2015, **21**, 11972; (i) S. Saha, J. Bachl, T. Kundu, D. Díaz Díaz and R. Banerjee, *Chem. Commun.*, 2014, **50**, 3004; (j) L. Jiang, Y. Yan and J. Huang, *Soft Matter*, 2011, **7**, 10417; (k) Z. Xu, J. Peng, N. Yan, H. Yu, S. Zhang, K. Liu and Y. Fang, *Soft Matter*, 2013, **9**, 1091; (l) J. Yan, J. Liu, P. Jing, C. Xu, J. Wu, D. Gao and Y. Fang, *Soft Matter*, 2012, **8**, 11697.
- (a) H. Maeda, *Chem. - A Eur. J.*, 2008, **14**, 11274; (b) S. Banerjee, R. K. Das and U. Maitra, *J. Mater. Chem.*, 2009, **19**, 6649; (c) Z. Qi, P. M. de Molina, W. Jiang, Q. Wang, K. Nowosinski, A. Schulz, M. Grzdzelski and C. A. Schalley, *Chem. Sci.*, 2012, **3**, 2073.
- (a) Y. Hisamatsu, S. Banerjee, M. B. Avinash, T. Govindaraju and C. Schmuck, *Angew. Chem., Int. Ed.*, 2013, **52**, 12550; (b) J. Nanda, A. Biswas and A. Banerjee, *Soft Matter*, 2013, **9**, 4198.
- S.-I. Kawano, N. Fujita, S. Shinkai, *J. Am. Chem. Soc.*, 2004, **126**, 8592.
- C. D. Jones and J. W. Steed, *Chem. Soc. Rev.*, 2016, **45**, 6546.
- (a) E. Carretti, M. Bonini, L. Dei, B. H. Berrie, L. V. Angelova, P. Baglioni and R. G. Weiss, *Acc. Chem. Res.*, 2010, **43**, 751; (b) A. Dawn, T. Shiraki, S. Haraguchi, S. -I. Tamaru and S. Shinkai, *Chem. Asian J.*, 2011, **6**, 266.
- (a) C. Wang, Q. Chen, F. Sun, D. Zhang, G. Zhang, Y. Huang, R. Zhao and D. Zhu, *J. Am. Chem. Soc.*, 2010, **132**, 3092; (b) Y. Lin, Y. Qiao, P. Tang, Z. Li and J. Huang, *Soft Matter*, 2011, **7**, 2762.
- (a) J. Eastoe, M. Sánchez-Dominguez, P. Wyatt and R. K. Heenan, *Chem. Commun.*, 2004, 2608; (b) P. Xue, J. Ding, M. Jin and R. Lu, *J. Mater. Chem. C*, 2017, **5**, 5299.
- S. Mondal, P. Chakraborty, P. Bairi, D. P. Chatterjee and A. K. Nandi, *Chem. Commun.*, 2015, **51**, 10680.

- 12 (a) S. Wang, W. Shen, Y. Feng and H. Tian, *Chem. Commun.*, 2006, 1497; (b) J. W. Chung, S. -J. Yoon, S. -J. Lim, B. -K. An and S. Y. Park, *Angew. Chem., Int. Ed.*, 2009, 48, 7030.
- 13 D. Chang, W. Yan, Y. Yang, Q. Wang and L. Zou, *Dyes Pigm.*, 2014, 110, 2.
- 14 (a) A. Y. -Y. Tam and V. W. -W. Yam, *Chem. Soc. Rev.*, 2013, 42, 1540; (b) M. -O. M. Piepenbrock, G. O. Lloyd, N. Clarke and J. W. Steed, *Chem. Rev.*, 2010, 110, 1960; (c) J. H. Lee, S. Kang, J. Y. Lee and J. H. Jung, *Soft Matter*, 2012, 8, 6557; (d) K. Lalitha, V. Sridharan, C. U. Maheswari, P. K. Vemula and S. Nagarajan, *Chem. Commun.*, 2017, 53, 1538; (e) K. Jie, Y. Zhou, B. Shi and Y. Yao, *Chem. Commun.*, 2015, 51, 8461; (f) S. Banerjee, N. N. Adarsh and P. Dastidar, *Soft Matter*, 2012, 8, 7623; (g) A. Ghossoub and J. -M. Lehn, *Chem. Commun.*, 2005, 5763; (h) S. Datta and S. Bhattacharya, *Soft Matter*, 2015, 11, 1945.
- 15 W. Edwards and D. K. Smith, *Chem. Commun.*, 2012, 48, 2767.
- 16 Q. Jin, L. Zhang, X. Zhu, P. Duan and M. Liu, *Chem. - A Eur. J.*, 2012, 18, 4916.
- 17 A. A. Sobczuk, S. -I. Tamarua and S. Shinkai, *Chem. Commun.*, 2011, 47, 3093.
- 18 A. Gasnier, G. Royal and P. Terech, *Langmuir.*, 2009, 25, 8751.
- 19 W. Deng and D. H. Thompson, *Soft Matter*, 2010, 6, 1884.
- 20 (a) K. Sawada and Y. Kikuchi, *Bunseki Kagaku.*, 2004, 53, 1239; (b) B. Tümmeler, G. Maass, E. Weber, W. Wehner and F. Vögtle, *J. Am. Chem. Soc.*, 1977, 99, 4683; (c) C. Xu, W. Liu and W. Qin, *J. Phys. Chem. A.*, 2011, 115, 4288.
- 21 (a) G. W. Gokel, *Crown Ethers and Cryptands.*, Royal Society of Chemistry: London, 1991; (b) Y. Suzuki, T. Morozumi and H. Nakamura, *J. Phys. Chem. B.*, 1998, 102, 7910.
- 22 (a) J. Kim, T. Morozumi, H. Hiraga and H. Nakamura, *Anal. Sci.*, 2009, 25, 1319; (b) H. Hiraga, T. Morozumi and H. Nakamura, *Eur. J. Org. Chem.*, 2004, 4680; (c) T. Morozumi, T. Anada and H. Nakamura, *J. Phys. Chem. B.*, 2001, 105, 2923; (d) H. Hiraga, T. Morozumi and H. Nakamura, *Tetrahedron Lett.*, 2002, 43, 9093; (e) J. Kim, T. Morozumi, N. Kurumatani and H. Nakamura, *Tetrahedron Lett.*, 2008, 49, 1984; (f) J. Kim, T. Morozumi and H. Nakamura, *Chem. Lett.*, 2009, 38, 994; (g) J. Kim, T. Morozumi, and H. Nakamura, *Org. Lett.*, 2007, 9, 4419.
- 23 (a) E. N. W. Howe, M. Bhadbhade and P. Thordarson, *J. Am. Chem. Soc.*, 2014, 136, 7505; (b) A. Bajaj, P. Kondaiah and S. Bhattacharya, *Bioconjugate Chem.*, 2007, 18, 1537; (c) S. Bhattacharya and A. Bajaj, *J. Phys. Chem. B.*, 2007, 111, 2463; (d) S. Bhattacharya and Y. Krishnan-Ghosh, *Mol. Cryst. Liq. Cryst.*, 2002, 381, 33.
- 24 (a) A. Reddy, A. Sharma and A. Srivastava, *Chem. - A Eur. J.*, 2012, 18, 7575; (b) S. D. Bhagat and A. Srivastava, *CrystEngComm.*, 2016, 18, 4369.
- 25 D. Perrin, W. L. F. Armarego and D. R. Perrin, *Purification of Laboratory Chemicals, 2nd Ed.*, Oxford: Pergamon 1980.
- 26 H. T. A. Merck, *J. Comput. Chem.*, 1996, 17, 490.
- 27 S. Profeta and N. L. Allinger, *J. Am. Chem. Soc.*, 1985, 107, 1907.
- 28 T. A. Halgren, *J. Comput. Chem.*, 1996, 17, 490.
- 29 *Spartan 08*, Software, Wavefunction Inc: Irvine, CA, USA, 2008.
- 30 A. D. Becke, *Phys. Rev. A*, 1988, 38, 3098.
- 31 C. Lee, W. Yang and R. G. Parr, *Phys. Rev. B.*, 1988, 37, 785.
- 32 G. A. Petersson and M. A. Al-Laham, *J. Chem. Phys.*, 1991, 94, 608.
- 33 A. V. Marenich, C. J. Cramer and C. J. Truhlar, *J. Phys. Chem. B.*, 2009, 113, 6378.
- 34 M. J. Frisch, G. W. Trucks, H. B. Schlegel, G. E. Scuseria, M. A. Robb, J. R. Cheeseman, G. Scalmani, V. Barone, B. Mennucci, G. A. Petersson, et al., *Gaussian 09, Revision B01*, Gaussian, Inc., Wallingford, CT, 2010. DOI: 10.1039/C8SM01071D
- 35 (a) Y. Wang, P. Xing, S. Li, M. Ma, M. Yang, Y. Zhang, B. Wang and A. Hao, *Langmuir.*, 2016, 32, 10705; (b) J. Nanda and A. Banerjee, *Soft Matter*, 2012, 8, 3380; (c) R. Misra, A. Sharma, A. Shiras and H. N. Gopi, *Langmuir.*, 2017, 33, 7762.
- 36 (a) H. Kar, D. W. Gehrig, N. K. A. G. Fernández, F. Laquai and S. Ghosh, *Chem. Sci.*, 2016, 7, 1115; (b) T. Mondal, T. Sakurai, S. Yoneda, S. Seki and S. Ghosh, *Macromolecules.*, 2015, 48, 879.
- 37 (a) H. Agarwalla, K. Jana, A. Maity, M. K. Kesharwani, B. Ganguly and A. Das, *J. Phys. Chem. A.*, 2014, 118, 2656; (b) M. Gangopadhyay, A. Maity, A. Dey and A. Das, *J. Org. Chem.*, 2016, 81, 8977; (c) F. Ali, S. Saha, A. Maity, N. Taye, M. K. Si, E. Suresh, B. Ganguly, S. Chattopadhyay and A. Das, *J. Phys. Chem. B.*, 2015, 119, 13018; (d) M. Gangopadhyay, A. K. Mandal, A. Maity, S. Ravindranathan, P. R. Rajamohanam and A. Das, *J. Org. Chem.*, 2016, 81, 512; (e) M. Suresh and A. Das, *Tetrahedron Lett.*, 2009, 50, 5808.



327x160mm (300 x 300 DPI)